

Cosmic Chemical Evolution

Renyue Cen¹ and Jeremiah P. Ostriker²

Received _____; accepted _____

¹Princeton University Observatory, Princeton University, Princeton, NJ 08544;
cen@astro.princeton.edu

²Princeton University Observatory, Princeton University, Princeton, NJ 08544;
jpo@astro.princeton.edu

ABSTRACT

Numerical simulations of standard cosmological scenarios have now reached the degree of sophistication required to provide tentative answers to the fundamental question: Where and when were the heavy elements formed? Averaging globally, these simulations give a metallicity that increases from 1% of the solar value at $z = 3$ to 20% at present. This conclusion is, in fact, misleading, as it masks the very strong dependency of metallicity on local density. At every epoch higher density regions have much higher metallicity than lower density regions. Moreover, the highest density regions quickly approach near solar metallicity and then saturate, while more typical regions slowly catch up. These results are much more consistent with observational data than the simpler picture (adopted by many) of gradual, quasi-uniform increase of metallicity with time.

Subject headings: Cosmology: large-scale structure of Universe – cosmology: theory – intergalactic medium – quasars: absorption lines – hydrodynamics

1. Introduction

One of the greatest successes of the Big Bang theory is that its prediction that the primordial baryonic matter is almost entirely composed of hydrogen and helium with a trace amount of a few other light elements is in detailed agreement with current observations (e.g., Schramm & Turner 1998). The heavier elements, collectively called “metals”, are thought to be made at much later times through nucleosynthesis in stars. Metals are ubiquitous in the universe in virtually all environments that have been observed, including regions outside of galaxies, the intergalactic medium (“IGM”), ranging from the metal rich intracluster medium to low metallicity Lyman alpha clouds. However, metallicity (the ratio of the amount of mass in metals to the total baryonic mass for a given region, $M_{\text{metals}}/M_{\text{baryons}}$, divided by 0.02 for the Sun, Z_{\odot}) is observed to be very variable. For example, metallicity reaches as high as ten (in units of the solar value, where value unity corresponds to $M_{\text{metals}}/M_{\text{baryons}} = 2\%$) in central regions of active galactic nuclei (Mushotsky, Done, & Pounds 1993; Hamann 1997; Tripp, Lu, & Savage 1997) but is as low as 10^{-3} for some halo stars in our own galaxy (Beers 1999). Disparity in metallicity values is also seen at high redshift. For instance, metallicity in damped Ly α systems is as high as 0.5 and as low as 0.01 at redshift $z \sim$ (Prochaska & Wolfe 1997), whereas it is about 0.01 in moderate column density Ly α clouds at $z \sim 3$ (Tytler et al. 1995; Songaila & Cowie 1996). Low column density Lyman alpha clouds at $z \sim 2 - 3$ appear to have still lower metallicity (Lu et al. 1998; Tytler & Fan 1994).

The question that naturally rises then is: When were the metals made and why are they distributed as observed? Can we understand the strong dependence of Z/Z_{\odot} on the gas density (at redshift zero) and the comparable dependence of Z/Z_{\odot} on redshift for regions of a given overdensity? While these are well-posed questions, addressing them directly is a formidable computational problem and requires both a large dynamic range,

to ensure a fair piece of the universe to be modeled, and sufficiently realistic physics being modeled including gasdynamics, galaxy formation, galactic winds and metal enrichment. After years of continuous improvement of both numerical techniques and physical modeling, coupled with rapid increase in computer power, we have now reached the point where this important question can at last be addressed in a semi-quantitative fashion using numerical simulations.

2. Model

The results reported on here are based on a new computation of the evolution of the gas in a cold dark matter model with a cosmological constant; the model is normalized to both the microwave background temperature fluctuations measured by COBE (Smoot et al. 1992) on large scales (Bunn & White 1997) and the observed abundance of clusters of galaxies in the local universe (Cen 1998), and it is close to both the concordance model of Ostriker & Steinhardt (1995) and the model indicated by the recent high redshift supernova results (Reiss et al. 1998). The relevant model parameters are: $\Omega_0 = 0.37$, $\Omega_b = 0.049$, $\Lambda_0 = 0.63$, $\sigma_8 = 0.80$, $H_0 = 70\text{km/s/Mpc}$, $n = 0.95$ and 25% tensor mode contribution to the CMB fluctuations on large scales. Two simulations with box sizes of $L_{box} = (100, 50)h^{-1}\text{Mpc}$ are made, each having 512^3 cells and 256^3 dark matter particles with the mean baryonic mass in a cell being $(1.0 \times 10^8, 1.3 \times 10^7)h^{-1} M_\odot$ and the dark matter particle mass being $(5.3 \times 10^9, 6.6 \times 10^8)h^{-1} M_\odot$, respectively, in the two simulations. Output was rescaled to $\Omega_b = 0.037$ to match latest observations (Burles & Tytler 1998). The results shown are mostly based on the large box, while the small box is used to check resolution effects.

The description of the numerical methods of the cosmological hydrodynamic code and input physical ingredients can be found elsewhere (Cen & Ostriker 1999a,b). To briefly recapitulate, we follow three components separately and simultaneously: dark matter, gas

and galaxies, where the last component is created continuously from the former two during the simulations in places where real galaxies are thought to form, as dictated mostly by local physical conditions. Self-consistently, feedback into IGM from young stars in the “galaxies” is allowed, in three related forms: supernova thermal energy output, UV photon output and mass ejection from the supernova explosions. The model reproduces the observed UV background as a function of redshift and the redshift distribution of star formation (“Madau Plot”; Nagamine, Cen & Ostriker 1999), among other diagnostics. Metals are followed as a separate variable (analogous to the total gas density) with the same hydrocode. We did not fit to the observed distributions and evolution of metals, but assumed a specific efficiency of metal formation. Subsequently rescaling the computed results to an adopted “yield” (Arnett 1996), the percentage of stellar mass that is ejected back into IGM as metals, of 0.02 (from an input value 0.06).

A word about the resolution of the simulation is appropriate here. The conclusions drawn in this paper are not significantly affected by the finite resolution, as verified by comparing the two simulations. Let us give an argument for why this is so. Although our numerical resolution is not sufficient to resolve any internal structure of galaxies, the resolution effect should affect different regions with different large-scale overdensities more or less uniformly since our spatial resolution is uniform and our mass resolution is good even for dwarf galaxies. In other words, galaxy formation in our simulations is not significantly biased against low density regions. Thus, the distribution of the identified galaxies as a function of large-scale overdensity in the simulation would be similar, if we had a much better resolution. It is the distribution of the galaxies that determines the distribution of metals, which is the subject of this paper. Needless to say, we can not make detailed modeling of the ejection of metals from galaxies into the IGM and this ignorance is hidden in the adopted “yield” coefficient. However, once the metals get out of galaxies, their dynamics is followed accurately. Changing the adopted yield by some factor would change

all quoted metallicities by the same factor but not alter any statements about spatial and temporal distribution of metals.

3. Results

Figure 1 shows the evolution of metallicity averaged over the entire universe (dot-dashed curve) and four regions with four different overdensities, $\delta_\rho = (10^3, 10^2, 20, 0)$, smoothed by a Gaussian window of size $0.3h^{-1}\text{Mpc}$, respectively, that approximately correspond to clusters of galaxies, Lyman limit and damped $\text{Ly}\alpha$ systems, moderate column density $\text{Ly}\alpha$ clouds and very low column density $\text{Ly}\alpha$ clouds, at $z = (3, 1.0, 0.5, 0)$. Note that a given class of objects is chosen to have a fixed comoving overdensity, not to have a fixed physical density. This choice is made because the decrease (of a factor 10 or so) of the observed meta-galactic radiation field from $z \sim 3$ to $z \sim 0$, and the increase of the size of structure with time at a fixed comoving density approximately compensate for the decrease in comoving density so a fixed comoving density approximately corresponds to a fixed column density at different redshift. This applies for the last three classes of objects. For the first class of objects (clusters of galaxies) either choice gives comparable results, due to the fact that metallicity saturates at the highest density (see below).

Several trends are clear. First, metallicity is a strong function of overdensity in the expected sense: high density regions have higher metallicity. Second, and more surprisingly, the evolution of metallicity itself is a strong function of overdensity: high density regions evolve slowly with redshift, whereas the metallicity in low density regions decreases rapidly towards high redshift. Finally, the overall metallicity evolution averaged globally differs from that of any of the constituent components. Therefore *any given set of cosmic objects (including stars or $\text{Ly}\alpha$ forest) cannot be representative of the universal metallicity at all times*, although at a given epoch one may be able to identify a set of objects that has

metallicity close to the universal mean. For example, at $z = 3$, regions with overdensity 20 (which roughly correspond to Lyman alpha clouds of column density of $\sim 10^{14.0-15.0} \text{ cm}^{-2}$) have metallicities very close to the global mean, while at $z = 0$, regions with overdensity of one hundred (which roughly correspond to Lyman limit and damped Lyman alpha systems) has metallicity very close to the global mean.

It has been the conventional wisdom to expect that, as all “metals” are produced (but not, on balance, destroyed) by stars, the metal abundance should increase with time or decrease with increasing redshift. What we see from Figure 1 is that there is another trend which is as strong as or stronger than this. Since stars are *relatively* overabundant in the densest regions, metallicity is a strongly increasing function of density at any epoch. This trend is observed within galaxies (with central parts being most rich) but it is also true when one averages over larger regions. The gas in dense clusters of galaxies is far more metal rich than the general IGM at $z = 0$. This trend is shown in another way in Figure 2, where metallicity is plotted as a function of overdensity at four redshifts.

Let us now examine the individual components more closely in Figure 3 with panels (a,b,c,d) showing the metallicity distributions for regions of overdensity $(10^3, 10^2, 20, 0)$, respectively, at four redshifts $z = (3, 1, 0.5, 0)$. We examine each panel in turn. In panel (a) we see that there is almost no evolution from redshift zero (thick solid curve) to redshift one (dotted curve) for metallicity of intracluster gas. The narrowness of the computed distributions fits observations very well for clusters locally and at low redshift. But we predict that the metallicity of clusters at redshift $z = 3$ will be somewhat lower than their low redshift counterparts by a factor of about three, with the characteristic metallicity declining to $Z \sim 0.1 Z_{\odot}$.

Second, examining panel (b) for regions with overdensity 10^2 , which roughly correspond to Lyman limit and damped Lyman alpha systems, it is seen that the median metallicity

increases only slightly from $z = 3$ to $z = 0.5$, but there is a large range of metallicity expected of approximately 30 at any redshift, in very good agreement with observations over the entire redshift range considered.

Next, panel (c) shows the integral distributions for regions with overdensity 20, that correspond to moderate column density Lyman alpha clouds with column density $10^{14} - 10^{15} \text{cm}^{-2}$. We see that the median metallicity increases by a factor of about 10 from redshift $z = 3$ to $z = 0$, but with a broad tail towards the low metallicity end at all redshift, again in good agreement with observations. Davé et al. (1998) concluded that the metallicity for regions of overdensity of ~ 10 at $z \sim 3$ is $10^{-2.5}$ from analysis of CIV absorption lines, consistent with our results here.

Finally, panel (d) shows regions with overdensity 0 (i.e, at the mean density) corresponding to the very low column density Lyman alpha clouds. The observations are upper bounds. But it appears that the bulk of the regions with such low density indeed has quite low metallicity, consistent with observations. Davé et al. (1998) derived an upper bound on metallicity for near mean density region at $z \sim 3$ of 10^{-3} from analysis of OVI absorption lines, in agreement with our results.

4. Conclusion

In the simulation examined in this paper high density regions reach an approximately solar density first, with lower density regions approaching that level at later epochs, and at all epochs the variations of Z with density is comparable to or larger than the variations at a given overdensity. This saturation of metallicity has a natural physical explanation. Regions where the peaks of long and short waves fortuitously coincide have the highest initial overdensity and the earliest significant star formation; but, when the long waves

break, high temperature shocks form (as in the centers of clusters of galaxies), so that further new galaxy formation and infall onto older systems ceases, star formation declines (Blanton et al. 1999), and the metallicity stops increasing. Observationally, we know that, in the highest density, highest metallicity and highest temperature regions of the rich clusters of galaxies, new star formation has essentially ceased by redshift zero. As a side note, that fact that metallicity depends as strongly on density as on time implies that stellar metallicity need not necessarily (anti-)correlate with the stellar age. For example, young stars may be relatively metal poor, as supported by recent observations (Preston, Beers & Sheckman 1994; Preston 1994), simply because these young stars may have formed out of relatively lower density regions where metallicity was low.

The picture presented here is, in principle, quite testable. For example, Steidel and co-workers (Steidel 1993; Steidel et al. 1994) and Savage et al. (1994) and others have found that metal line systems observed along a line of sight to a distant quasar are invariably associated with galaxies near the line of sight at the redshift of the metal line system. One would expect, on the basis of the work presented here, that there would be a strong statistical trend associating higher metallicity systems to closer galaxies, since for these the typical overdensity is larger. Figure 4 shows surface density contours on a slice of $50 \times 50 \times 10h^{-3}\text{Mpc}^3$ for galaxies (filled red; at a surface density of 31 times the mean surface density of galaxies), metals (green; at a metallicity of $0.16 Z_{\odot}$) and warm/hot gas (Cen & Ostriker 1999a) with $T = 10^5 - 10^7\text{K}$ (blue; at a surface density of 6.8 times the mean surface density of warm/hot gas). Each respective contour contains 90% of the total mass of the respective component. We see that most of the green contours contain red spots, each within a region of size approximately $1h^{-1}\text{Mpc}$; i.e., one would expect to see a normal galaxy associated with a metal line system within a projected distance of $\sim 1h^{-1}\text{Mpc}$. It is also seen from Figure 4 that metal rich gas is generally embedded in the warm/hot gas. This may manifest itself observationally as spectral features that seem to arise from

multiple phase gas at a similar redshift along the line of sight. Recent observations appear to have already hinted this; Lopez et al. (1998), using combined observations of quasar absorption spectra from Hubble Space Telescope and other ground-based telescopes, noted that some C IV clouds are surrounded by large highly ionized low-density clouds. Finally, it may be pointed out that most of the metals are in over-dense regions and these regions are generally relatively hot: $> 10^5$ Kelvin. Therefore, they should be observable in the EUV and soft X-ray emitting warm/hot gas (Cen & Ostriker 1999a).

The work is supported in part by grants NAG5-2759 and AST93-18185, ASC97-40300. We thank Ed Jenkins, Rich Mushotzky, Jim Peebles, David Spergel, Michael Strauss and Todd Tripp for discussions.

REFERENCES

- Arnaud, K.A., Mushotzky, R.F., Ezawa, H., Fukazawa, Y., Ohashi, T., Bautz, M.W., Crewe, G.B., Gendreau, K.C., Yamashita, K., Kamata, Y., & Akimoto, F. 1994, ApJ, 436, L67 (A94)
- Arnett, D. 1996, “Supernovae and Nucleosynthesis”
- Bahcall, N.A., & Cen, R. 1992, ApJ, 407, L49
- Barlow, T.A., & Tytler, D. 1998, AJ, 115, 1725 (BT98)
- Blanton, M., Cen, R., Ostriker, J.P., & Strauss, M.A. 1999, ApJ, in press
- Bunn, E.F., & White, M. 1997, ApJ, 480, 6
- Burles, S., & Tytler, D. 1998, ApJ, 499, 699
- Cen, R. 1998, ApJ, 509, 16
- Cen, R., & Ostriker, J.P. 1998a, ApJ, in press (preprint, astro-ph/9809370)
- Cen, R., & Ostriker, J.P. 1999b, in preparation
- Davé, R., Hellsten, U., Hernquist, L., Weinberg, D.H., & Katz, N. 1998, ApJ, 487, 482
- Hamann, F. 1997, ApJS, 109, 279
- Lu, L., Sargent, W.L.W., Barlow, T.A., Churchill, C.W., & Vogt, S.S. 1996, ApJS, 107, 475 (Lu96)
- Lu, L., Sargent, W.L.W., Barlow, T.A., & Rauch, M. 1998, preprint, astro-ph/9802189 (Lu98)
- Mushotzky, R.F., Done, C., & Pounds, K.A. 1993, ARAA, 31, 717

- Mushotzky, R.F., & Lowenstein, M. 1997, ApJ, 481, L63 (ML97)
- Mushotzky, R.F., Lowenstein, M., Arnaud, A.K., Tamura, T., Fukazawa, Y., Matsushita, K., Kikuchi, K., & Hatsukade, I. 1996, ApJ, 466, 686 (M96)
- Nagamine, K., Cen, R., & Ostriker, J.P. 1999, in preparation
- Ostriker, J.P., & Steinhardt, P. 1995, Nature, 377, 600
- Pettini, M., Ellison, S.L., Steidel, C.C., & Bowen, D.V. 1998, preprint, astro-ph/9808017 (P98)
- Prochaska, J.X., & Wolfe, A.M. 1998, ApJ, in press (PW98)
- Prochaska, J.X., & Wolfe, A.M. 1997, ApJ, 474, 140 (PW97)
- Rauch, M., Haehnelt, M.G., & Steinmetz, M. 1997, ApJ, 481, 601 (R97)
- Reiss, A.G., et al. 1998, preprint, astro-ph/9805201
- Savage, B.D., Tripp, T.M., & Lu, L. 1998, AJ, 115, 436
- Schramm, D.N., & Turner, M.S. 1998, Rev. Mod. Phys., 70, 303
- Shull, J.M., et al. 1998, preprint, astro-ph/9807246 (S98)
- Smoot, G.F., et al. 1992, ApJ, 396, L1
- Songaila, A., & Cowie, L.L. 1996, AJ, 112, 335 (SC96)
- Steidel, C.C. 1993, in “The Environment and Evolution of Galaxies”, ed. J.M. Shull and H.A. Thronson, Jr., p263
- Steidel, C.C., Dickinson, M., & Persson, S.E. 1994, ApJ, 437, L75

- Tamura, T., Day, C.S., Fukazawa, Y., Hatsukade, I., Ikebe, Y., Makishima, K., Mushotzky, R.F., Ohashi, T., Takenaka, K., & Yamashita, K. 1996, PASP, 48, 671 (T96)
- Tripp, T. M., Lu, L., & Savage, B. D. 1997, AJ, 112, 1
- Tytler, D., Fan, X.-M., Burles, S., Cottrell, L., Davis, C., Kirkman, D., & Zuo, L. 1995, in QSO Absorption Lines, ed. G. Meylan (Berlin: Springer), 289
- Tytler, D., & Fan, X.-M. 1994, ApJ, 424, L87 (TF94)
- White, S.D.M, Navarro, J., Evrard, A.E., & Frenk, C.S. 1993, Nature, 366, 429

Fig. 1.— The average metallicities averaged over the whole universe (dot-dashed curve), overdensity 10^3 (thick solid curve), overdensity 10^2 (thin solid curve), overdensity 10 (dotted curve) and overdensity 0 (dashed curve), respectively, as a function of redshift.

Fig. 2.— The average metallicities as a function of overdensity at four redshifts. The variances are 1σ .

Fig. 3.— Panel (a) shows the differential metallicity distribution for regions with overdensity 10^3 (clusters of galaxies) at four different redshifts, $z = 0$ (thick solid curve), $z = 0.5$ (thin solid curve), $z = 1$ (dotted) and $z = 3$ (dashed curve) [the same convention will be used for panels (b,c,d)]. Also shown as symbols are observations from various sources. Various symbols are observations: the open circle from Mushotzky & Lowenstein (1997; ML97) showing that there is almost no evolution in the intracluster metallicity from $z = 0$ to $z \sim 0.3$ at around one-third of solar, the open triangles from from Mushotzky et al. (1996; M96) showing the metallicities of four individual nearby clusters (Abell 496, 1060, 2199 and AWM 7), the open square from Tamura et al. (1996; T96) showing the metallicity of the intracluster gas of Abell 1060, the filled triangle from Arnaud et al. (1994; A94) showing the metallicity of the intracluster gas of the Perseus cluster. All metallicities are measured in $[\text{Fe}/\text{H}]$. Panel (b) shows the differential metallicity distribution for regions with overdensity 10^2 . The open triangle from Lu et al. (1996; Lu96) shows the result from an extensive analysis of a large database of damped Lyman alpha systems with $0.7 < z < 4.4$. The horizontal range on the open triangle does not indicate the errorbar on the mean rather it shows the range of metallicities of the observed damped Lyman alpha systems as given by Lu96. The open circle from Pettini et al. (1998; P98) is due to an analysis of ten damped Lyman alpha systems at $z < 1.5$; here the horizontal range indicates the error on the mean. The open square due to Prochaska & Wolfe (1998; PW98) is from an analysis of 19 damped Lyman alpha systems at $z > 1.5$; the horizontal range indicates the error on the mean.

Finally, the two solid dots are from Prochaska & Wolfe (1997; PW97) of an analysis of two damped Lyman alpha systems at $z \sim 2.0$ with one having extreme low metallicity and the other having extreme high metallicity. All metallicities are measured in $[\text{Zn}/\text{H}]$. Vertical position in panel (b) is without significance. Panel (c) shows the cumulative metallicity distribution for regions with overdensity 20. The symbols are observations: the open circle from SC96⁶ for Lyman alpha clouds at $z \sim 3$ with column density of $N > 3 \times 10^{14} \text{cm}^{-2}$, the open triangle from Rauch et al. (1997; R97) for Lyman alpha clouds at $z \sim 3$ with column density of $N > 3 \times 10^{14} \text{cm}^{-2}$, the solid dot from Barlow & Tytler (1998; BT98) for Lyman alpha clouds at $z \sim 0.5$ with column density of $N > 3 \times 10^{14} \text{cm}^{-2}$, the solid triangle from Shull et al. (1998; S98) for Lyman alpha clouds at $z \sim 0$ with column density of $N = (3 - 10) \times 10^{14} \text{cm}^{-2}$. Panel (d) shows the cumulative metallicity distribution for regions with overdensity 0 (i.e., mean density). The open circle is the upper limit for Lyman clouds with column density $N = 10^{13.5} - 10^{14.0} \text{cm}^{-2}$ at redshift $z = 2.2 - 3.6$ from Lu et al. (1998; Lu98). The open triangle is the upper limit for Lyman clouds with column density $N = 10^{13.0} - 10^{14.0} \text{cm}^{-2}$ at redshift $z \sim 3$ from Tytler & Fan (1994; TF94). The model seems consistent with observations of low column density Lyman alpha clouds at high redshift.

Fig. 4.— Surface density contours on a slice of $50 \times 50 \times 10 h^{-3} \text{Mpc}^3$ for galaxies (filled red; at a surface density of 31 times the mean surface density of galaxies), metals (green; at a metallicity of $0.16 Z_{\odot}$) and warm/hot gas¹² with $T = 10^5 - 10^7 \text{K}$ (blue; at a surface density of 6.8 times the mean surface density of warm/hot gas). Each respective contour contains 90% of the total mass of the respective component.

Figure 1

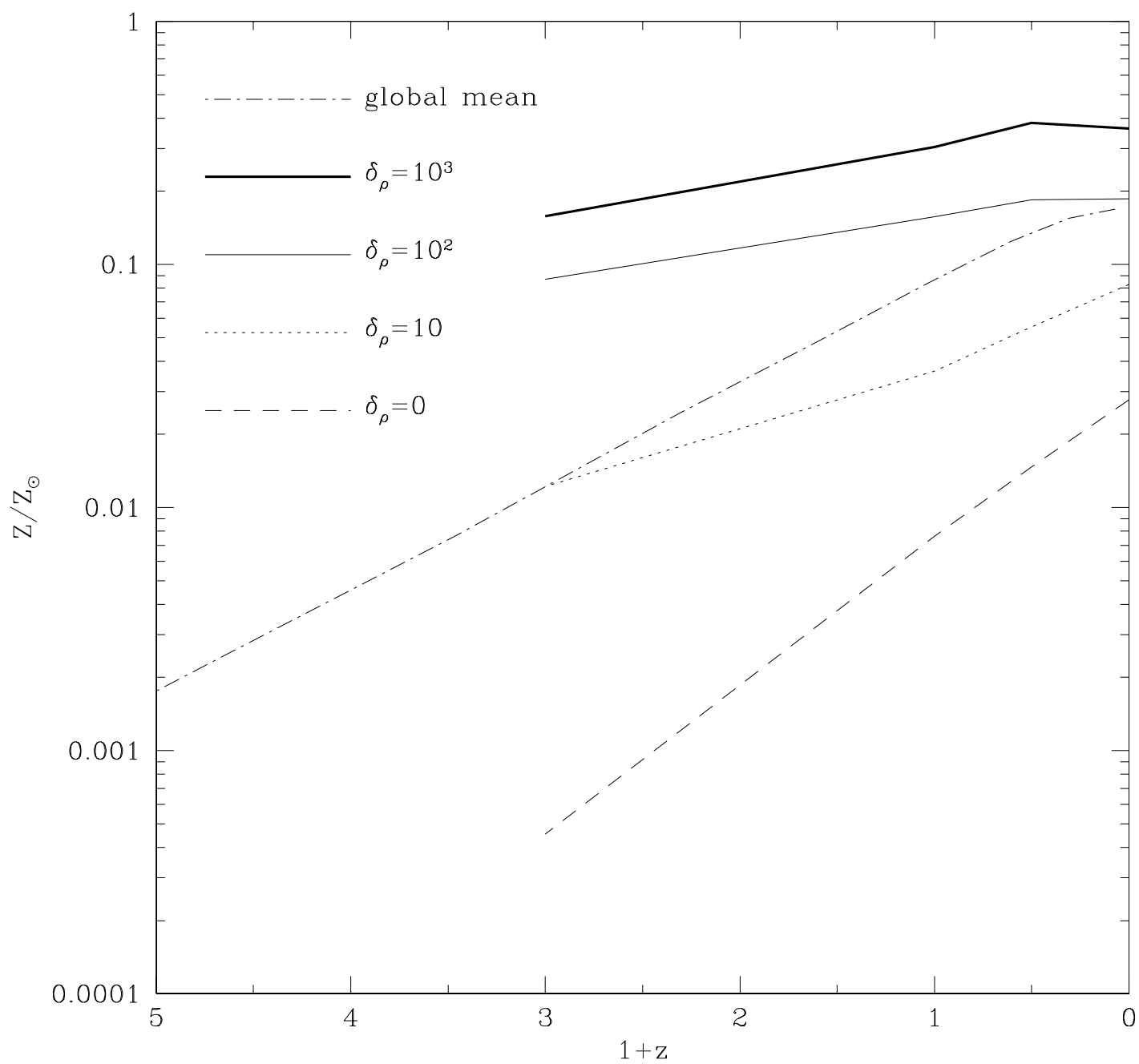


Figure 2

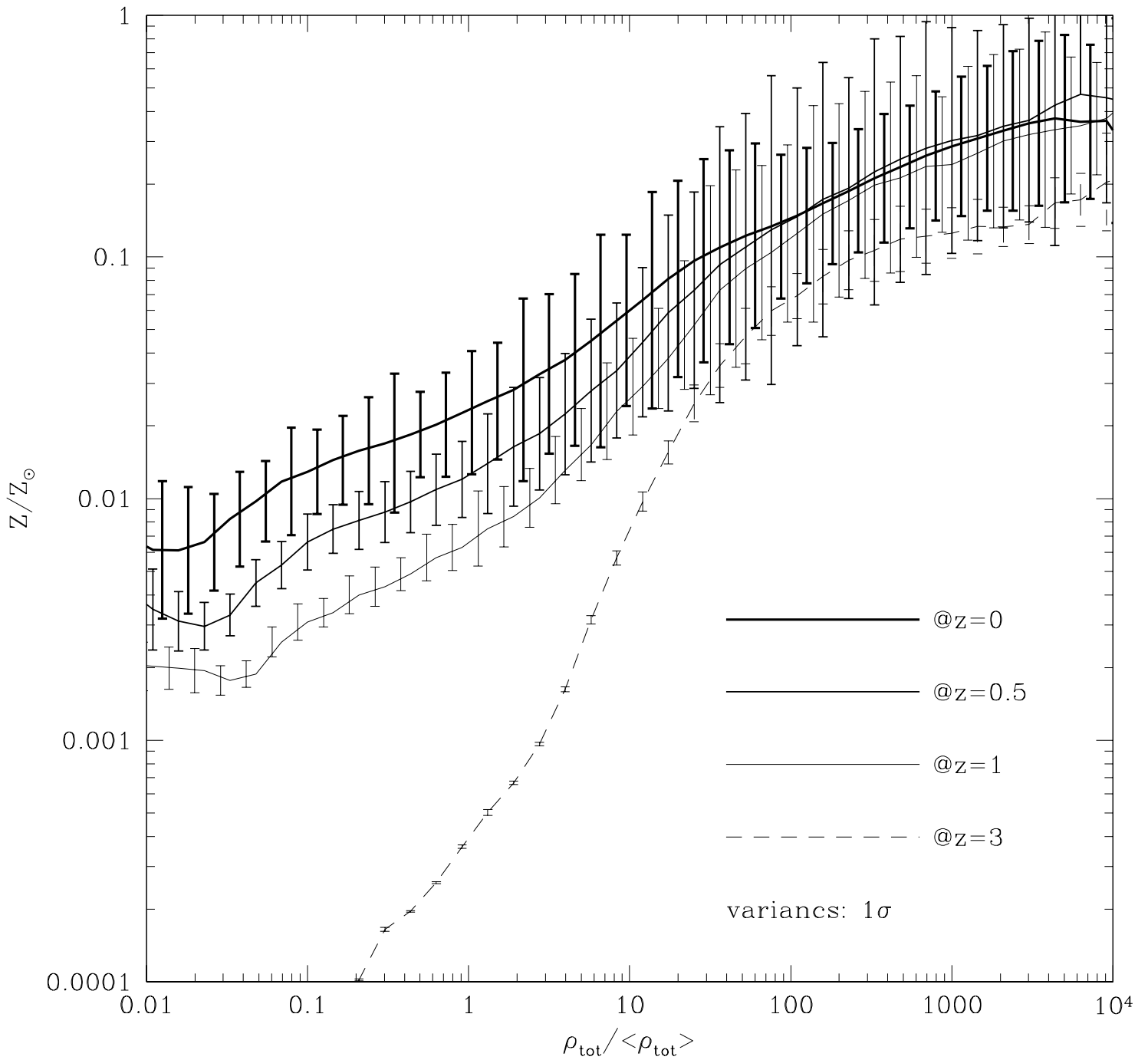


Figure 3

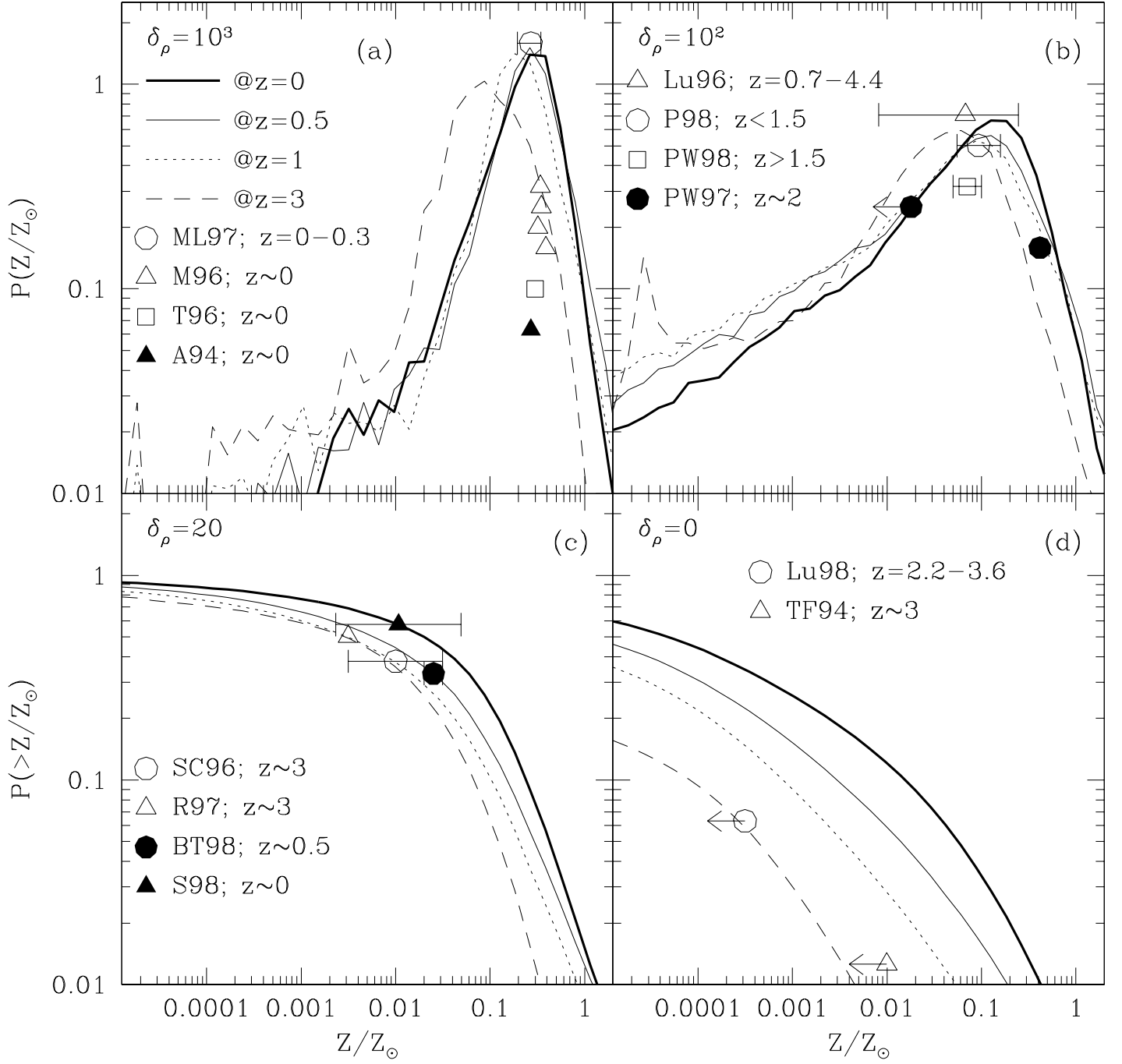


Figure 4

